PHYSICAL REVIEW B **90**, 155428 (2014)

Understanding intercalation structures formed under graphene on Ir(111)

Mie Andersen,[*] Liv Hornekær, and Bjørk Hammer
Interdisciplinary Nanoscience Center (iNANO) and Department of Physics and Astronomy, Ny Munkegade, Building 1520, Aarhus University, DK-8000 Aarhus C, Denmark

(Received 30 July 2014; revised manuscript received 29 September 2014; published 16 October 2014)

The coverage-dependent intercalation of oxygen, CO, hydrogen, alkali metals, and halogens between graphene and Ir(111) is investigated using density functional theory with van der Waals corrections. By comparing adsorption on clean Ir to intercalation we show that the presence of the graphene layer shifts the stability of the adsorption structures towards higher coverages, with oxygen as the only exception preferring low-coverage intercalation structures. In general, we find that the preferred adsorption site of the intercalant is important for the stability of intercalation structures, where an atop adsorption site favors higher-coverage structures compared to a hollow adsorption site. Overall, the predicted stable intercalation structures are in good agreement with experimentally observed intercalation structures. We calculate doping levels of intercalated graphene and show that there is a correlation between the amount of charge transfer to or from the graphene sheet and the graphene binding energy, which is an indication for ionic bonding between the graphene sheet and the intercalants. We show that the graphene doping level can be tuned almost continuously between strong *n*-type doping for the alkali metals and strong *p*-type doping for F. Further, we calculate C 1*s* core-level shifts for intercalated graphene and show that these are correlated with the calculated doping level. The obtained values for graphene doping levels and core-level shifts are qualitatively in good agreement with available experimental values, but we find quantitative disagreements of up to 0.3 eV.

DOI: 10.1103/PhysRevB.90.155428 PACS number(s): 71.15.Mb, 68.43.Fg, 73.22.Pr

I. INTRODUCTION

Epitaxial growth of graphene has been established as an important and efficient synthesis method. In the last decade, various growth strategies have been explored, ranging from the thermal decomposition of SiC surfaces [1,2] to chemical vapor deposition on catalytically active surfaces, including metals [3–5] and recently also semiconductors such as *h*-BN and Ge [6–8]. A major advantage of such growth methods is that they enable the efficient production of wafer-scale graphene flakes [9], often exhibiting excellent crystalline quality [5,8].

Further studies on epitaxial graphene have focused on tailoring the graphene-substrate interaction as well as the graphene electronic properties by the intercalation of atoms or molecules such as oxygen [10–14], hydrogen [15,16], CO [17–19], alkali metals [14,20–23], and halogen atoms [24–26]. In this way, so-called quasi-free-standing graphene has been produced, characterized by a very low electronic and geometric perturbation from the underlying substrate [11,14,15]. Further, it has been established that the doping level of the graphene can be controlled depending on the intercalated atom or molecule [10–12,14,18,21–24,26], which could have important implications for graphene electronics. For graphene grown on metals, the intercalation-mediated decoupling from the underlying metal has allowed for fundamental studies of many-body effects in graphene [14] as well as the peeling of graphene flakes [25]. For graphene grown on SiC, the intercalation of hydrogen has proven very successful for turning the reconstructed initial carbon layer (the so-called buffer layer) into quasi-free-standing monolayer graphene owing to the saturation of the topmost Si atoms of the SiC surface with hydrogen [15].

Other studies have been devoted to the catalytic activity of the confined space between the metal and the graphene for fundamental reactions such as CO oxidation [17,27], Si oxidation [28], and H_2 oxidation [29]. It is well established that the placement of catalysts in confined spaces such as inside zeolites [30] or carbon nanotubes [31] can enhance the activity or selectivity of the catalyst. It is expected that the confinement effects of a graphene cover could similarly modify the catalytic properties of the underlying metal. A fundamental question to be answered in this context is whether the presence of the graphene sheet can allow for new structures of adsorbed atoms or molecules forming and/or modify the binding energies in such structures, all of which could have important implications for catalysis and materials science applications.

Here, we present a systematic study of the structures and stabilities of various intercalation systems formed under graphene on Ir(111) using density functional theory with van der Waals corrections. We investigate a broad range of experimentally relevant atoms and molecules covering oxygen, CO, hydrogen, alkali metals, and halogen atoms. The paper is organized as follows: The computational details are given in Sec. II. In Sec. III A, we investigate the coverage-dependent adsorption energies, comparing adsorption on the clean Ir(111) surface with intercalation between Ir and graphene. In Sec. III B, we explore further the doping and the core-level shifts for intercalated graphene. The conclusions are given in Sec. IV.

II. COMPUTATIONAL DETAILS

The density functional theory calculations were performed with the real-space projector augmented wave code

---

[*] mie.andersen@ch.tum.de

©2014 American Physical Society

GPAW [32] and the Atomic Simulation Environment (ASE) interface [33]. To account for van der Waals (vdW) interactions between the graphene sheet and the substrate, we employed the optB88-vdW functional [34], which has proven successful for similar systems such as graphene on Ni [35] and benzene adsorption on metals [36].

The Ir/graphene Moiré superstructure was approximated by a five-layered $(\sqrt{3} \times \sqrt{3})$ Ir slab to a 30° rotated (2×2) graphene layer since we, in a previous publication concerning O intercalation, have shown that choosing a smaller Ir/graphene superstructure leads to only minor changes in graphene binding energies and average graphene binding distances [14]. This elementary unit cell was repeated to a (3×3) supercell in order to accommodate the $(3\sqrt{3} \times 3\sqrt{3})R30^\circ$-19CO intercalation structure and the 0.04-ML CO intercalation structure with only one CO in the supercell, whereas the remaining intercalation structures could be accommodated either in the elementary unit cell (for coverages of 0.33, 0.67, or 1 ML) or in the (2×2) supercell (for remaining coverages). Coverages are given with respect to the number of Ir surface atoms. The **k**-point sampling was (6×6) for the elementary unit cell, (4×4) for the (2×2) supercell, and (2×2) for the (3×3) supercell for the structural optimizations and energies, whereas the density of states calculations required **k**-point samplings of (36×36), (18×18), and (12×12) for the three respective cell sizes.

The graphene lattice constant was fixed to its optimized value of 2.465 Å and the Ir lattice constant was adapted accordingly, resulting in a strain of 2.76%. In the relaxation, the bottom Ir layer was kept fixed, while all other atoms were relaxed until the maximum force on each atom was below 0.02 eV/Å. Two-dimensional (2D) periodic boundary conditions were employed parallel to the surface, and a vacuum region of 6 Å separated any atom from the cell boundaries perpendicular to the surface. The grid spacing was 0.185 Å.

Some adsorption structures for Li and Cl were found using a genetic algorithm [37,38]. For the initial screening of adsorption structures, we used two-layered Ir slabs, an LCAO basis set, and gamma point **k**-point sampling. We used a set of 20 starting candidates and a population size of 20. New structures were generated using the cut-and-splice operator and 15% of the generated structures were mutated using either the rattle or mirror mutation as described in Ref. [38]. For each coverage around 70–100 different structures were tested. The 20 most favorable structures were then further optimized using three-layered Ir slabs, a grid-based basis set, and (2×2) **k**-point sampling. We note that the use of a genetic algorithm allows for a structure search unbiased by any expectations or experimental knowledge.

Throughout the paper, we give adsorption potential energies for adsorption on clean Ir $E_{\text{ads,Ir}}$ according to the formula

$$E_{\text{ads,Ir}} = (E_{\text{Ir/ads}} - E_{\text{Ir}} - n * E_{\text{ads}})/n, \qquad (1)$$

where $E_{\text{Ir/ads}}$ is the energy of the adsorption structure, E_{Ir} is the energy of the clean Ir slab, n is the number of atoms or molecules in the adsorption structure, and E_{ads} is the energy of the isolated adsorbate. For CO, this is the energy of a CO molecule in the gas phase, whereas for the remaining adsorbates this is half of the energy of the diatomic molecule in the gas phase. Correspondingly, we give adsorption potential energies for intercalation between graphene and Ir $E_{\text{ads,int}}$ according to the formula

$$E_{\text{ads,int}} = (E_{\text{Ir/ads/gr}} - E_{\text{Ir/gr}} - n * E_{\text{ads}})/n, \qquad (2)$$

where $E_{\text{Ir/ads/gr}}$ is the energy of the intercalation structure and $E_{\text{Ir/gr}}$ is the energy of nonintercalated graphene on Ir. Graphene binding energies are given according to the formula

$$E_{\text{b}} = (E_{\text{Ir/ads}} + E_{\text{gr}} - E_{\text{Ir/ads/gr}})/m, \qquad (3)$$

where E_{gr} is the energy of the isolated graphene layer and m is the number of C atoms in the graphene layer. Note that with this convention adsorption potential energies are negative numbers whereas graphene binding energies are positive numbers.

The C 1s core-level shifts (CLSs) of intercalated graphene on Ir were calculated relative to nonintercalated graphene on Ir to compare with experimental measurements. In practice, this was done by calculating the shift of a C atom in the graphene layer relative to a reference C atom adsorbed on the backside of the five-layered Ir slab for both the nonintercalated and the intercalated graphene. The subtraction of these relative shifts then cancels out the effect of the artificial reference atom and allows for comparing CLSs between different computational supercells. Where necessary, the CLSs of C atoms in different local environments within the graphene layer were averaged. With the used sign convention, a positive CLS corresponds to a shift to higher binding energies in the experiment. The fully screened core-hole approximation was used, meaning that the self-consistent total energy of the system including the core hole was evaluated. Thus, final-state effects were taken into account.

Since convergence problems were encountered for some CLS calculations with the optB88-vdW functional, we chose to calculate all CLSs with the PBE functional based on the geometries optimized with optB88-vdW after checking that the two functionals give very similar results. CLSs calculations can be slightly functional dependent, however, e.g., the use of the M06-L functional for calculating the CLS of the 0.50-ML O intercalation structure gives a value of −0.40 eV [29], which is somewhat more negative than the optB88-vdW/PBE value of −0.28 eV.

III. RESULTS AND DISCUSSION

A. Coverage dependence

We begin by comparing the coverage-dependent adsorption on clean Ir(111) to the intercalation between graphene and Ir. In Fig. 1, we plot the adsorption potential energy as a function of the coverage for oxygen, CO, hydrogen, and Li, where Li is chosen as a representative for the alkali metals.

For O on clean Ir(111) experimental studies have shown that the dissociative adsorption of O_2 at saturation coverage leads to the formation of rotated domains with a defective $p(2 \times 1)$-O structure where the O atoms are adsorbed in the fcc hollow sites [39,40]. Here, we compare three different O structures: a low-coverage (0.08-ML) structure [cf. Fig. 2(a)], the 0.25-ML $p(2 \times 2)$-O structure [cf. Fig. 2(b)], and the 0.50-ML $p(2 \times 1)$-O structure [cf. Fig. 2(c)]. The adsorption potential energies are plotted in Fig. 1(a) and are also given in Table I. In agreement with a previous computational study [41], we find on the clean Ir surface that the potential energy increases (corresponding

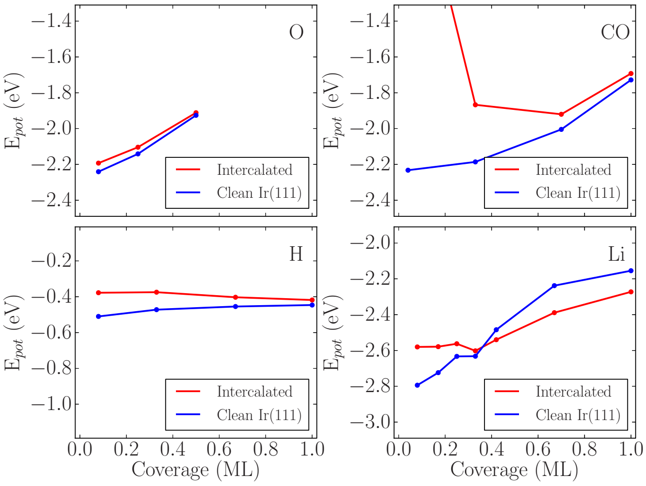

FIG. 1. (Color online) Adsorption potential energies comparing adsorption on clean Ir(111) to intercalation between graphene and Ir for O, CO, H, and Li as a function of the adsorbate coverage. E_{pot} refers to either $E_{\text{ads,Ir}}$ or $E_{\text{ads,int}}$ as defined in Eqs. (1) and (2).

to a decrease in stability) when the O coverage is increased from 0.25 to 0.50 ML. In the same study, the authors found also an increase in potential energy for coverages lower than 0.25 ML. This is in disagreement with our results, where the lowest potential energy is found at low coverage. As a check, we repeated the calculations using the PBE functional and the optimized Ir lattice constant, which still gives us the most stable O adsorption structure at low coverage.

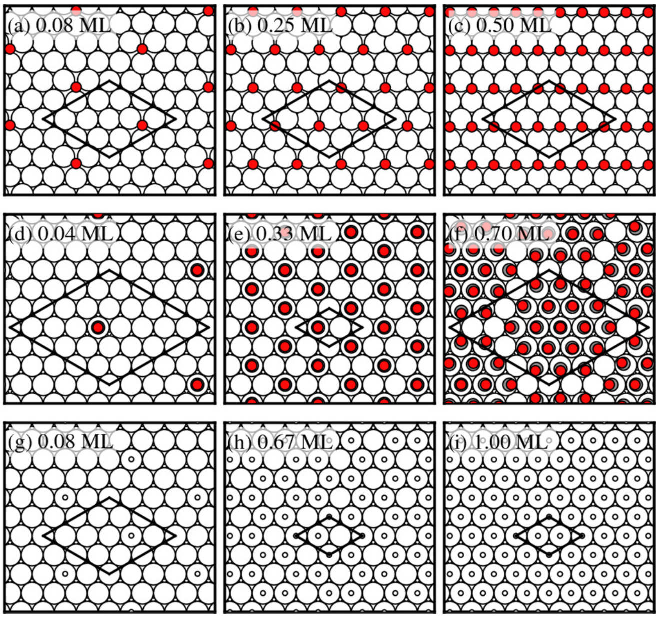

FIG. 2. (Color online) Adsorbate structures on Ir(111) at various coverages for (a)–(c) O, (d)–(f) CO, and (g)–(i) H. Ir atoms are shown as large white spheres, O and C atoms are shown as medium red and gray spheres, respectively, and H atoms are shown as small white spheres. The unit cells employed for describing the Ir/adsorbate/graphene intercalation structures are outlined in black. They are all multiples of the elementary unit cell consisting of a $(\sqrt{3}\times\sqrt{3})$ Ir slab to a 30° rotated (2 × 2) graphene layer.

TABLE I. Considered coverages Θ (in ML), adsorption potential energies per atom or molecule for adsorption on clean Ir $E_{\text{ads,Ir}}$ (in eV) and intercalated between Ir and graphene $E_{\text{ads,int}}$ (in eV), intercalation energies ΔE_{int} (defined as $E_{\text{ads,int}} - E_{\text{ads,Ir}}$) (in eV), graphene binding energies E_{b} (in meV/C), and average graphene binding distances d_{av} (in Å) comparing nonintercalated Ir/graphene to intercalated Ir/graphene for various atoms and molecules. For O, CO, Li, and Cl, different coverages are compared.

	Θ	$E_{\text{ads,Ir}}$	$E_{\text{ads,int}}$	ΔE_{int}	E_{b}	d_{av}
None					63	3.48
O	0.08	−2.24	−2.19	0.05	62	3.56
O	0.25	−2.14	−2.10	0.04	60	3.81
O	0.50	−1.93	−1.91	0.02	60	4.05
CO	0.33	−2.19	−1.87	0.32	22	6.22
CO	0.70	−2.00	−1.92	0.08	40	6.12
CO	1.00	−1.73	−1.69	0.04	49	6.10
H	1.00	−0.45	−0.42	0.03	52	4.26
Li	0.08	−2.79	−2.58	0.21	56	3.86
Li	0.33	−2.63	−2.60	0.03	59	4.20
Li	1.00	−2.15	−2.27	−0.12	107	4.32
Na	0.33	−2.06	−2.05	0.01	61	5.06
K	0.33	−2.21	−2.27	−0.06	70	5.76
Rb	0.33	−2.18	−2.24	−0.06	69	6.04
Cs	0.33	−2.35	−2.37	−0.02	65	6.40
F	1.00	−2.49	−2.61	−0.12	110	4.69
Cl	0.33	−1.93	−1.70	0.23	33	5.15
Cl	0.58	−1.76	−1.70	0.06	49	5.41
Br	0.33	−1.98	−1.74	0.24	33	5.37
I	0.33	−2.12	−1.88	0.24	33	5.77

In the presence of the graphene layer, we observe that the O adsorption potential energies do not change much, and that the low-coverage adsorption structure is still most favorable. We speculate that this is a result of the relatively small size of the O atom and the fact that it adsorbs in the hollow site, which potentially makes the perturbation of the graphene binding to the substrate very small. In Table I, we compare the binding of graphene on the clean Ir surface to the binding when O is present. It is seen that the binding is not much perturbed at any O coverage. Experimentally, O intercalation between graphene and Ir was studied in Refs. [11,12] using XPS, STM, and ARPES. In good agreement with the present calculations, it was found that O initially forms a dilute intercalation structure followed by the more dense $p(2\times2)$-O and $p(2\times1)$-O structures at increased exposure.

At ultrahigh vacuum conditions, low-energy electron diffraction (LEED) experiments have revealed that CO forms $(\sqrt{3}\times\sqrt{3})R30^\circ$-CO or $(2\sqrt{3}\times2\sqrt{3})R30^\circ$-7CO structures on Ir(111) depending on the exposure [39,42]. At millibar pressures [18], or when CO is adsorbed from a CO-saturated 0.1-M HClO4 solution [43], a higher-coverage $(3\sqrt{3}\times3\sqrt{3})R30^\circ$-19CO structure has been identified using STM. Both experiments and calculations [44] agree that CO adsorbs in the atop position. We consider here four representative CO structures: low (0.04-ML) CO coverage [cf. Fig. 2(d)], the 0.33-ML $(\sqrt{3}\times\sqrt{3})R30^\circ$-CO structure [cf. Fig. 2(e)], the 0.70-ML $(3\sqrt{3}\times3\sqrt{3})R30^\circ$-19CO structure [cf. Fig. 2(f)], and the 1-ML structure [similar to the 1-ML H structure shown

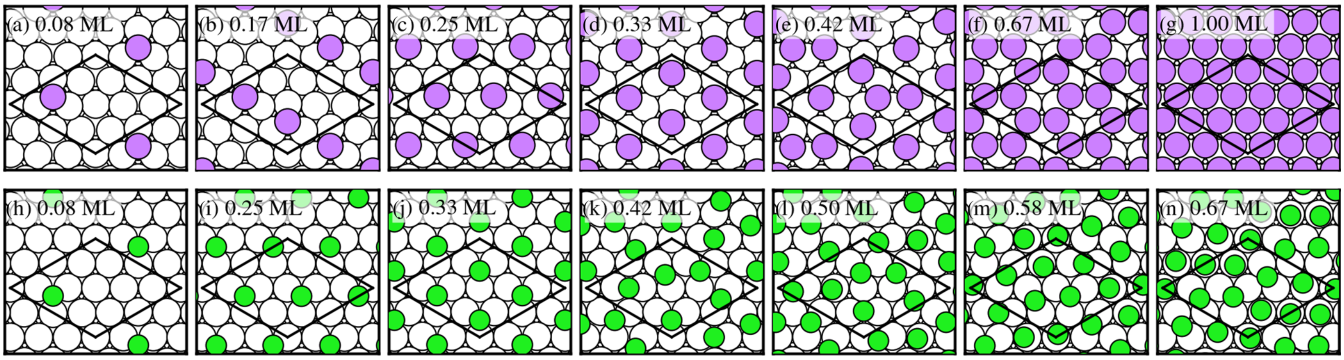

FIG. 3. (Color online) Adsorbate structures on Ir(111) at various coverages for (a)–(g) Li and for (h)–(n) Cl. Ir atoms are shown as white spheres, Li atoms as purple spheres, and Cl atoms as green spheres. The unit cells are outlined in black. The structures in (e) and in (k)–(n) have been found using a genetic algorithm.

in Fig. 2(i)]. The adsorption potential energies are plotted in Fig. 1(b). For adsorption on clean Ir it is seen that the potential energy increases monotonically with the coverage. This is in contrast to the intercalated situation, where it is most favorable to form the $(3\sqrt{3}\times 3\sqrt{3})R30^\circ$-19CO structure corresponding to a coverage of 0.70 ML. From a combined XPS and STM study [18] it was found that pressures in the millibar range are needed to intercalate CO under graphene on Ir(111), and the $(3\sqrt{3}\times 3\sqrt{3})R30^\circ$-19CO structure was identified as the only possible intercalation structure in good agreement with our results.

We speculate that the remarkable different coverage-dependent behavior for CO compared to O stems from the fact that CO is a larger rodlike molecule with a preferred atop adsorption site. For low-coverage intercalation structures, the graphene is lifted far away from the surface, and the resulting loss in graphene binding energy is divided out on a small number of molecules. This gives rise to very high adsorption potential energies for CO, which is reflected by the fact that CO in the 0.04-ML intercalation structure relaxes into a hollow site and adsorbs with a tilted angle in order to minimize the perturbation of the graphene-metal bonding (not shown). For the higher-coverage structures, the preferred adsorption site is atop like on clean Ir. For the most stable 0.70-ML intercalation structure, the graphene binding energy is reduced from 63 meV/C in the nonintercalated case to 40 meV/C atom in the intercalated case (cf. Table I).

H adsorption on Ir(111) was studied with high-resolution electron-energy-loss spectroscopy (HREELS) [45] and with density functional theory (DFT) calculations at 0.25-ML coverage [44]. Both studies agree that the preferred adsorption site is atop. Here, we consider four H coverages: low (0.08-ML) H coverage [cf. Fig. 2(g)], the 0.33-ML $(\sqrt{3}\times\sqrt{3})R30^\circ$-H structure [similar to the 0.33-ML CO structure shown in Fig. 2(e)], the 0.67-ML $(\sqrt{3}\times\sqrt{3})R30^\circ$-2H structure [cf. Fig. 2(h)], and the 1-ML structure [cf. Fig. 2(i)]. The adsorption potential energies are plotted in Fig. 1(c). In agreement with the previous studies, we find that the most favorable adsorption site on clean Ir is atop. This is also the case for the intercalated structures, except for the lowest considered coverage of 0.08 ML, where the fcc hollow site is preferred similar to what was found for CO. In general, the variation of the H binding with the coverage is very small, and this is in particular true for the intercalated structures. The difference between the H binding energy at 0.67 and 1 ML is only 15 meV/H, with the 1-ML structure being the most stable. Experimentally, H intercalation under graphene on Ir(111) was studied with XPS and STM [16], and the coverage was determined to be 0.82 ML. This agrees well with our finding of favorable H adsorption energies over a wide range of high-coverage structures. In the 1-ML intercalated structure, the graphene binding is reduced to 52 meV/C (cf. Table I).

The intercalation of alkali metals has been considered in several experimental studies. For K [46] and Cs [23] LEED studies have revealed $(\sqrt{3}\times\sqrt{3})$ patterns with respect to Ir or (2×2) patterns with respect to graphene, which with our choice of Ir/graphene supercell corresponds to the same structure at a coverage of 0.33 ML. For Na [47] and Li [23] also higher-coverage structures have been observed at increased exposures, e.g., Li exhibits a range of coverages all the way up to 1 ML.

For all of the alkali metals we find that the hcp hollow site is the preferred adsorption site both on clean Ir and for the intercalated structures. In Fig. 1(d), we plot the adsorption energies for Li in the coverage range 0.08 to 1 ML. We tested different configurations of the Li atoms to obtain the most stable structure at each coverage. For the 0.42-ML structure, a full genetic algorithm search was performed as described in Sec. II since no obvious regular adsorption pattern would fit into the chosen Ir/graphene supercell. The resulting most stable structures are shown in Figs. 3(a)–3(g). It is seen that all Li atoms adsorb in hcp hollow sites, i.e., for the 0.42-ML structure it is for example not favorable to occupy different adsorption sites in order to distribute the Li atoms more evenly on the surface. The fact that the adsorption structures at different coverages do not all have a regular adsorption pattern is partly responsible for the observed slight disturbance from a smoothly increasing energy curve with the coverage on clean Ir. We note that the 0.33-ML structure is particularly stable compared to similar coverages (e.g., 0.25 ML), even though both structures form a regular adsorption pattern.

For the intercalated structures, the general trend is that low-coverage structures are preferred with the structure at 0.33 ML being slightly more stable (22 meV/Li) than the 0.08-ML structure. Still, the full monolayer structure is also quite stable. We calculate the differential adsorption potential energy for

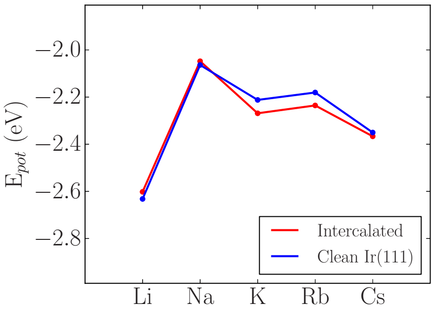

FIG. 4. (Color online) Adsorption potential energies comparing adsorption on clean Ir(111) to intercalation between graphene and Ir for the alkali metals Li, Na, K, Rb, and Cs at a coverage of 0.33 ML. E_{pot} is defined as in Fig. 1.

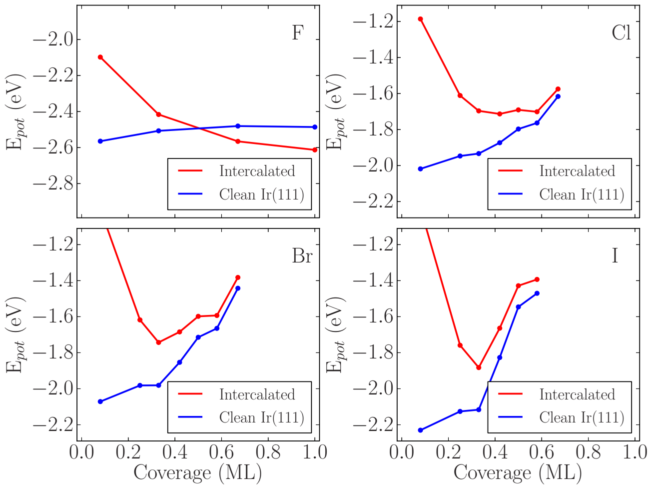

FIG. 5. (Color online) Adsorption potential energies comparing adsorption on clean Ir(111) to intercalation between graphene and Ir for F, Cl, Br, and I as a function of the adsorbate coverage. E_{pot} is defined as in Fig. 1.

the last four Li atoms to be added when increasing the coverage from 0.67 to 1 ML to be −2.04 eV/atom. This large negative number rationalizes the experimental observation that higher coverages can be achieved at increased exposure similar to what is observed for O, but we note that also changes in entropy and kinetic factors will influence the coverages achievable in the experiment.

In Fig. 4, we compare adsorption energies for the five considered alkali metals Li, Na, K, Rb, and Cs at a coverage of 0.33 ML since this is the most favorable coverage for all alkali metals (only showed for Li) and also the only experimentally observed coverage for the larger alkali metals K and Cs. An interesting observation is that for the larger alkali metals (K, Rb, and Cs), the adsorption potential energy is lower in the intercalated structure than it is on clean Ir, i.e., the intercalation is more favorable than the adsorption on clean Ir. This is reflected in the graphene binding energy, which correspondingly becomes larger in the intercalated structures (65–70 meV/C) than it is for nonintercalated graphene on Ir (63 meV/C) (cf. Table I). Also, for the 1-ML coverage Li-intercalated structure the graphene binding is significantly increased to 107 meV/C.

Next, we consider the intercalation of halogens. Experimentally, the intercalation of Cl was achieved by exposure to $FeCl_3$ [26]. Based on XPS measurements, the saturated amount of intercalated Cl atoms was found to be around 35% of the C atoms in the graphene. With our choice of Ir/graphene supercell, this corresponds to a coverage of 0.93 ML with respect to Ir. LEED measurements showed no sign of an ordered structure of the intercalated Cl. Also, the intercalation of Br has been achieved by exposure to Br_2 vapor [25]. No attempt was made to quantify the amount of intercalated Br, but it was observed that the mechanical exfoliation of graphene using adhesive tapes was greatly facilitated after intercalation. This was interpreted as a weakening of the graphene binding to the substrate.

In Fig. 5, we plot the coverage-dependent adsorption potential energy for F, Cl, Br, and I, comparing adsorption on clean Ir to intercalation. It turns out that F behaves qualitatively different from the other halogens and from O, its neighbor in the periodic table. The covalent radii of F and O are very similar and they are both very electronegative atoms. Therefore, one might intuitively expect a similar intercalation behavior, however, this turns out not to be the case. The main difference between the two atoms is that O adsorbs in the fcc hollow site, whereas F adsorbs in the atop site. It is seen that the adsorption potential energy of F on clean Ir is only weakly increasing with the coverage [cf. Fig. 5(a)] in contrast to the behavior of O [cf. Fig. 1(a)]. Here, the considered adsorption structures for F are the same as the ones for H shown in Figs. 2(g)–2(i). One explanation for the pronounced difference between F and O could be that the atop adsorption site makes F less sensitive to repulsive interactions at high coverage since neighboring F atoms do not share bonding to the same Ir atom.

Also in the intercalated case the adsorption site makes a large difference. Similar to what was observed for CO and H, the preferred atop adsorption site for F makes low-coverage intercalated structures very unfavorable with the F atom in the 0.08-ML structure preferring to move into the fcc hollow site. Like for H the full monolayer intercalated structure is most favorable. Similar to what was observed for the alkali metals, the F atom is bound stronger in the most favorable intercalated structure than in the corresponding adsorption structure on clean Ir, and correspondingly the graphene binding energy is significantly increased to 110 meV/C (cf. Table I).

For the remaining halogens Cl, Br, and I, the preferred adsorption site is the fcc hollow site. We consider coverages ranging from 0.08 up to 0.67 ML (Cl and Br), and 0.58 ML (I). Even though a very high maximum coverage of intercalated Cl (0.93 ML) was proposed in Ref. [26] we do not include this coverage, as it leads to very high Cl adsorption potential energies. We will return to this point under the discussion of CLSs in Sec. III B. Similar to the approach followed for Li, we used a genetic algorithm to determine the most favorable structures for the coverages larger than 0.33 ML, where no obvious regular adsorption pattern would fit into the chosen Ir/graphene supercell. The resulting structures are shown in Figs. 3(h)–3(n). Since the energetics for occupying different adsorption sites is similar for Cl, Br, and I, we performed only a full genetic algorithm search for Cl, and the obtained most favorable structures were employed also for Br and I. The resulting coverage-dependent adsorption potential energies are plotted in Figs. 5(b)–5(d).

On clean Ir, the adsorption potential energies are monotonically increasing with the coverage for all three halogens, however, the structures at 0.33 and 0.58 ML coverage appear to be slightly more stable compared to the general trend of a smoothly increasing energy curve. From an inspection of the structures in Figs. 3(h)–3(n) it is clear that the stabilization at 0.58 ML must be related to the fact that the atoms at this coverage can arrange themselves in a structure similar to a regular close-packed pattern within the chosen supercell. There is no obvious explanation for the increased stability at 0.33 ML since both this structure and the structure at 0.25 ML form regular patterns with all atoms adsorbed on the most favorable fcc hollow site. The interaction between the adsorbates at 0.33-ML coverage must therefore be particularly favorable similar to what was observed for Li.

In the intercalated case, the presence of the graphene layer shifts the most favorable structures towards higher coverages. For Cl, the potential energy curve is very broad with a range of intermediate coverages between 0.33 and 0.58 ML having comparable stability. For Br and I, the potential energy curve becomes increasingly narrow with the 0.33-ML structure being most stable. Presumably, this behavior originates from the increasing atomic size of Br and I, which make the adsorption potential energies raise more steeply with the coverage also on the clean Ir surface. In Table I, we compare the graphene binding energy at 0.33- and 0.58-ML coverage for Cl, and at 0.33-ML coverage for Br and I. At 0.33 ML, the graphene binding energy is weakened from 63 meV/C in the nonintercalated case to around 33 meV/C in the intercalated case for all three halogens, whereas for the Cl 0.58-ML structure, the reduction is a bit smaller. Such reductions of the graphene binding energy are in excellent agreement with the experimentally observed facilitation of graphene exfoliation caused by Br intercalation.

In order to give an accessible overview of the effect on the graphene binding for all the different intercalants and coverages considered, we give in Table I also the intercalation energy, which is the potential energy difference per atom or molecule between adsorption on clean Ir and intercalation for a given adsorption structure. A positive number means that the adsorption potential energy is lower on clean Ir than in the intercalated structure, and correspondingly intercalation reduces the graphene binding energy compared to nonintercalated graphene, and vice versa for negative numbers. In fact, there is a simple relationship between the intercalation energy E_{int} and the difference between the graphene binding energy in the intercalated and nonintercalated cases:

$$E_{\text{int}} = (E_{\text{b,nonint}} - E_{\text{b,int}}) * \frac{\#\text{C}}{\Theta * \#\text{Ir}}, \tag{4}$$

where $E_{\text{b,nonint}}$ and $E_{\text{b,int}}$ are the graphene binding energies for nonintercalated and intercalated graphene, #C is the number of C atoms in the graphene layer, Θ is the adsorbate coverage, and #Ir is the number of Ir surface atoms. In Table I, we give also the average Ir/graphene distance in the intercalation structures, which mainly reflects the size of the intercalant and the preferred adsorption site (atop adsorption site leads to a larger Ir/graphene distance than hollow adsorption site).

TABLE II. Considered coverages Θ (in ML), calculated graphene doping ΔV_{cal} (in eV), experimental graphene doping ΔV_{expt} (in eV), calculated core-level shifts CLS_{cal} (in eV), and experimental core-level shifts CLS_{expt} (in eV) comparing nonintercalated Ir/graphene to intercalated Ir/graphene for various atoms and molecules. For O, Li, and Cl, different coverages are compared.

	Θ	ΔV_{cal}	ΔV_{expt}	CLS_{cal}	CLS_{expt}
None		0.34	0.07[a]	≡ 0	≡ 0
O	0.08	0.34		−0.03	
O	0.25	0.41		−0.14	−0.34[c]
O	0.50	0.68	0.64[a]–0.80[b]	−0.28	−0.45[c]
CO	0.70	0.65		−0.23	−0.3[d]
H	1.00	0.50		−0.14	−0.14[e]
Li	0.08	−0.07		0.25	
Li	0.33	−0.82		0.70	
Li	1.00	−1.50	−1.6[f]	0.73	
Na	0.33	−0.90		0.77	
K	0.33	−0.97	−1.29[g]	0.79	
Rb	0.33	−0.97		0.79	
Cs	0.33	−0.95	−1.1[h]	0.77	
F	1.00	1.10		−0.83	
Cl	0.33	0.37		0.04	
Cl	0.58	0.65		−0.22	
Cl	0.93		0.6[h]		−0.33[h]
Br	0.33	0.23		0.18	
I	0.33	−0.06		0.32	

[a] Reference [11].
[b] Reference [14].
[c] Reference [12].
[d] Reference [18].
[e] Reference [16].
[f] Reference [23].
[g] Reference [46].
[h] Reference [26].

B. Doping and core-level shift

The control of the position of the graphene Dirac point has already been demonstrated in several experimental intercalation studies using ARPES. Whereas nonintercalated graphene on Ir(111) is slightly p doped, the intercalation of alkali metals such as Li [23], K [46], and Cs [23] leads to a rigid negative potential energy shift of the graphene π band levels with n-type dopings in the range −1.6 eV (1 ML Li) to −1.1 eV (0.33 ML Cs). Note that when giving *potential* energies n-type doping corresponds to a negative energy, whereas often in the literature ARPES results are quoted in terms of binding energies where n-type doping corresponds to a positive energy. For Cl intercalation, a p-type doping of 0.6 eV has been measured [26], and for O two different studies determined the p-type doping to be 0.64 [11] and 0.80 eV [14], where the latter value is probably related to a more complete O intercalation. The experimentally determined doping values are summarized in Table II. Further analysis of the intensity of the graphene π bands in O-intercalated graphene has

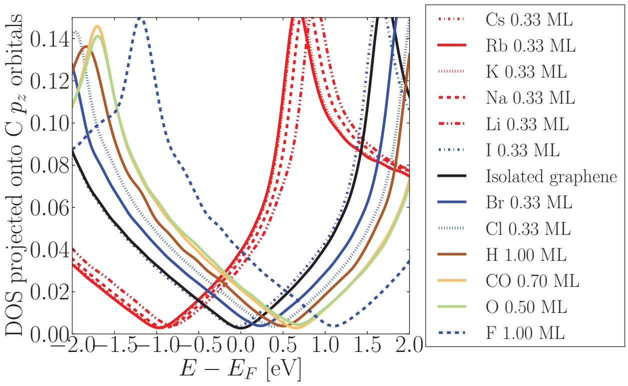

FIG. 6. (Color online) Density of states projected onto the C p_z orbitals comparing an isolated graphene sheet to graphene intercalated by various atoms and molecules. Different alkali or halogen atoms are distinguished by varying line styles, while they are plotted with the same line color.

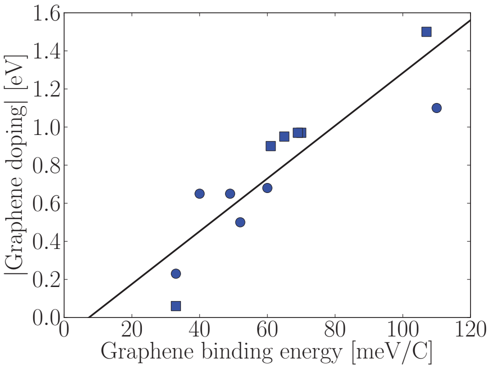

FIG. 7. (Color online) Correlation between calculated graphene binding energies and the absolute value of the calculated graphene doping for all considered intercalants at the maximal considered coverage. Intercalants giving rise to a positive (negative) doping are plotted with circles (squares).

revealed a decoupling from the Ir substrate characterized by the disappearance of substrate-related minigaps [11,14].

In Fig. 6, we plot the density of states projected onto the C p_z orbitals comparing an isolated graphene layer to intercalated graphene for F at 1-ML coverage, the remaining halogens and the alkali metals at 0.33-ML coverage, H at 1-ML coverage, O at 0.50-ML coverage, and CO at 0.70-ML coverage. It is seen that the shapes of the graphene π bands are very similar for intercalated and isolated graphene in good agreement with the experimentally observed rigid shift of the π system and the decoupling from the Ir surface. It is found that all intercalants decouple the graphene sheet from the Ir surface. Only at low coverage (e.g., 0.08-ML O) do we observe a modification of the graphene π bands (not shown) since here large parts of the graphene sheet interact directly with the Ir surface, leading to hybridization between the Ir d states and the graphene π bands. Such low coverages are, however, only relevant for O intercalation, as they are energetically unfavorable for all other intercalants. At the coverages considered in Fig. 6 we find that the alkali metals all give a similar n-type doping around −0.08 to −1 eV, whereas the halogens give very different doping levels ranging from slightly n-type doped (I) to a p-type doping of 1.10 eV (F). The intercalation of H, O, or CO all give similar p-type dopings of around 0.5–0.7 eV. In Table II, we summarize the calculated doping values and give also the coverage dependence for O, Li, and Cl.

For nonintercalated graphene, the calculated p-type doping (0.34 eV) exceeds the experimental value (0.07 eV) by 0.27 eV. For graphene intercalated with O or alkali metals, the calculated values are numerically around 0.1–0.3 eV lower than the experimental values. For Cl we consider the doping level at the calculated stable structure at 0.58-ML coverage instead of the experimentally determined 0.93-ML coverage. We find that the calculated doping level at 0.58-ML coverage (0.65 eV) exceeds the experimental doping level determined at 0.93-ML coverage (0.6 eV). We will come back to this point in the discussion of core-level shifts.

From a comparison of Tables I and II it is clear that the heavily n- or p-doped systems (1-ML F or Li) give rise to high graphene binding energies, whereas the systems with vanishing doping (e.g., 0.33-ML I) give rise to low graphene binding energies. In Fig. 7, we plot the correlation between the graphene binding energy and the absolute value of the calculated doping level. For O, Li, and Cl, we include only the maximal investigated coverage since for low coverage, the graphene binding is more dominated by the interaction with the Ir surface. Although the correlation is not perfect, it is clear that the general trend of increased graphene binding energy with increased degree of doping holds for all considered intercalation systems. This indicates that the nature of the bonding between the graphene and the intercalants is ionic, i.e., an intercalant that gives rise to a large charge transfer to or from the graphene sheet acts as an electrostatic glue between the graphene and the Ir substrate.

In several experimental studies it has been shown that the C 1s core-level shift (CLS) is useful for monitoring the intercalation of graphene. For O intercalation, the C 1s CLS was shown to change gradually from −0.17 eV for a dilute intercalation structure to −0.34 and −0.45 eV for the $p(2 \times 2)$-O and the $p(2 \times 1)$-O structures, respectively [12]. In contrast, CO intercalation yields only one value for the C 1s CLS at −0.3 eV [18], which corresponds to the dense $(3\sqrt{3} \times 3\sqrt{3})R30^\circ$-19CO structure. Further, H and Cl intercalation have been shown to give CLSs of −0.14 [16] and −0.33 eV [26], respectively.

CLSs were calculated as described in Sec. II and are compared to the available experimental values in Table II. For O and CO, the calculated CLSs are 0.07–0.2 eV less negative than the measured values, whereas for H the agreement is very good. For Cl, we consider again the calculated stable structures at 0.33- and 0.58-ML coverage instead of the experimentally determined 0.93-ML coverage. At 0.33 ML, we find a slightly positive CLS, whereas at 0.58 ML a value of −0.22 eV is reached, which is around 0.1 eV less negative than the measured CLS of −0.33 eV at 0.93-ML coverage. We note that our calculated doping level and CLS for 0.58-ML Cl coverage actually agree fairly well with the measured values, however, as previously discussed a coverage of 0.93 ML as determined in the experiment is not stable compared to the

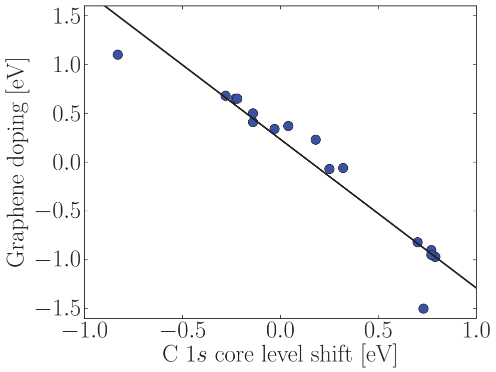

FIG. 8. (Color online) Correlation between calculated C 1s core-level shift and graphene doping for all considered intercalants and coverages.

Cl intercalation structures at 0.33- and 0.58-ML coverage. It is hence tempting to reconcile experiment and theory by assuming that the coverage was in fact lower than 0.93 ML in the experiment.

The alkali metals at 0.33-ML coverage all give very similar CLSs around 0.7–0.8 eV. For Li also the coverage dependence is given. Comparing the CLSs of Cl, Br, and I at 0.33-ML coverage we see that they become more positive as we move down the periodic table from 0.04 eV for Cl to 0.32 eV for I. Correspondingly, calculated doping levels for these three halogens start out positive for Cl (0.37 eV) and decrease for Br until a slightly negative value of −0.06 eV is reached for I. For F, a very negative CLS of −0.83 eV is obtained which is accompanied by a very positive calculated doping level of 1.10 eV. In Fig. 8, we plot the correlation between the calculated CLSs and doping levels for all considered intercalants and coverages. It is seen that the correlation is very good for all intermediate doping levels, whereas the largest *n*- or *p*-type doped structures (1-ML F or L) deviate somewhat from the general trend. The overall good correlation is a strong indication that the doping of the graphene sheet induced by the intercalants is one of the main factors determining the CLSs.

IV. CONCLUSIONS

We have investigated the coverage-dependent intercalation of oxygen, CO, hydrogen, alkali metals, and halogens, comparing adsorption on clean Ir to intercalation between graphene and Ir. In general, the presence of the graphene layer shifts the stability of the adsorption structures towards higher coverages as seen for CO, H, the halogens, and the alkali metals. O intercalation is a clear exception from this trend and we speculate that this is related to the small size of the atom and the fcc hollow adsorption site, which allows for dilute intercalation structures that hardly perturb the graphene binding. For the halogens, we showed that F behaves qualitatively different from the other halogens with slowly rising adsorption potential energies as a function of the coverage on clean Ir and a preferred intercalation structure of a full monolayer. In contrast, the remaining halogens preferred intermediate coverages, where their adsorption potential energy curves became progressively more narrow with increasing atomic size. In general, we find that the preferred adsorption site of the intercalants is important for the stability of the intercalation structures, where an atop adsorption site as found for F, H, and CO favors high-coverage intercalation structures close to a full monolayer, and a hollow adsorption site as found for O, the alkali metals, and the three halogens Cl, Br, and I favors low- or intermediate-coverage intercalation structures. On top of this, the atomic size of the intercalant is also important, where an increase in atomic size lowers the range of accessible intercalation coverages as found for the larger alkali metals and halogens. Overall, the predicted stable intercalation structures were in good agreement with experimentally observed intercalation structures.

In many cases, the intercalation leads to a weakening of the graphene binding, but important exceptions include the strongly doping F atom and the alkali metals, which can greatly enhance the graphene binding energy. We showed that there is a correlation between the calculated doping and the graphene binding energy, which is a strong indicator for ionic bonding between the graphene and the intercalants. On the other end of the scale, we identified intercalants such as Cl, Br, I, and to a lesser extent also CO and H, which gave up to a factor of 2 reduced binding energies in good agreement with the experimentally realized easy peeling of graphene flakes upon intercalation with Br.

Comparing the doping level of the graphene sheet intercalated by different atoms and molecules, we showed that the position of the Dirac point can be tuned almost continuously between strong *n*-type doping for Li and the other alkali metals and strong *p*-type doping, in particular observed for F. At the same time, the shape of the graphene bands remains similar to an isolated graphene layer in good agreement with the experimentally revealed decoupling of graphene from the substrate. Both the calculated doping levels and CLSs were in good qualitative agreement with the available experimental results, however, quantitative deviations of up to 0.3 eV were found. Finally, we showed that there is a correlation between calculated doping levels and CLSs for intercalated graphene, indicating that the doping level of the graphene layer is one of the main factors determining the CLS.

ACKNOWLEDGMENTS

Support from the Danish Council for Independent Research | Natural Sciences, The Lundbeck Foundation, and the Danish Center for Scientific Computing is acknowledged.

---

[1] K. V. Emtsev, A. Bostwick, K. Horn, J. Jobst, G. L. Kellogg, L. Ley, J. L. McChesney, T. Ohta, S. A. Reshanov, J. Röhrl, E. Rotenberg, A. K. Schmid, D. Waldmann, H. B. Weber, and T. Seyller, Nat. Mater. **8**, 203 (2009).

[2] C. Berger, Z. Song, X. Li, X. Wu, N. Brown, C. Naud, D. Mayou, T. Li, J. Hass, A. N. Marchenkov, E. H. Conrad, P. N. First, and W. A. de Heer, Science **312**, 1191 (2006).

[3] X. Li, W. Cai, J. An, S. Kim, J. Nah, D. Yang, R. Piner, A. Velamakanni, I. Jung, E. Tutuc, S. K. Banerjee, L. Colombo, and R. S. Ruoff, Science **324**, 1312 (2009).

[4] P. W. Sutter, J.-I. Flege, and E. A. Sutter, Nat. Mater. **7**, 406 (2008).

[5] J. Coraux, A. T. N'Diaye, C. Busse, and T. Michely, Nano Lett. **8**, 565 (2008).

[6] W. Yang, G. Chen, Z. Shi, C.-C. Liu, L. Zhang, G. Xie, M. Cheng, D. Wang, R. Yang, D. Shi, K. Watanabe, T. Taniguchi, Y. Yao, Y. Zhang, and G. Zhang, Nat. Mater. **12**, 792 (2013).

[7] M. Wang, S. K. Jang, W.-J. Jang, M. Kim, S.-Y. Park, S.-W. Kim, S.-J. Kahng, J.-Y. Choi, R. S. Ruoff, Y. J. Song, and S. Lee, Adv. Mater. **25**, 2746 (2013).

[8] J.-H. Lee, E. K. Lee, W.-J. Joo, Y. Jang, B.-S. Kim, J. Y. Lim, S.-H. Choi, S. J. Ahn, J. R. Ahn, M.-H. Park, C.-W. Yang, B. L. Choi, S.-W. Hwang, and D. Whang, Science **344**, 286 (2014).

[9] S. Bae, H. Kim, Y. Lee, X. Xu, J.-S. Park, Y. Zheng, J. Balakrishnan, T. Lei, H. R. Kim, Y. I. Song, Y.-J. Kim, K. S. Kim, B. Ozyilmaz, J.-H. Ahn, B. H. Hong, and S. Iijima, Nat. Nanotechnol. **5**, 574 (2010).

[10] P. Sutter, J. T. Sadowski, and E. A. Sutter, J. Am. Chem. Soc. **132**, 8175 (2010).

[11] R. Larciprete, S. Ulstrup, P. Lacovig, M. Dalmiglio, M. Bianchi, F. Mazzola, L. Hornekær, F. Orlando, A. Baraldi, P. Hofmann, and S. Lizzit, ACS Nano **6**, 9551 (2012).

[12] E. Grånäs, J. Knudsen, U. A. Schröder, T. Gerber, C. Busse, M. A. Arman, K. Schulte, J. N. Andersen, and T. Michely, ACS Nano **6**, 9951 (2012).

[13] S. Oida, F. R. McFeely, J. B. Hannon, R. M. Tromp, M. Copel, Z. Chen, Y. Sun, D. B. Farmer, and J. Yurkas, Phys. Rev. B **82**, 041411 (2010).

[14] S. Ulstrup, M. Andersen, M. Bianchi, L. Barreto, B. Hammer, L. Hornekær, and P. Hofmann, 2D Mater. **1**, 025002 (2014).

[15] C. Riedl, C. Coletti, T. Iwasaki, A. A. Zakharov, and U. Starke, Phys. Rev. Lett. **103**, 246804 (2009).

[16] E. Grånäs, T. Gerber, U. Schroeder, K. Schulte, J. N. Andersen, T. Michely, and J. Knudsen (unpublished).

[17] R. Mu, Q. Fu, L. Jin, L. Yu, G. Fang, D. Tan, and X. Bao, Angew. Chem. Int. Ed. **51**, 4856 (2012).

[18] E. Grånäs, M. Andersen, M. A. Arman, T. Gerber, B. Hammer, J. Schnadt, J. N. Andersen, T. Michely, and J. Knudsen, J. Phys. Chem. C **117**, 16438 (2013).

[19] L. Jin, Q. Fu, A. Dong, Y. Ning, Z. Wang, H. Bluhm, and X. Bao, J. Phys. Chem. C **118**, 12391 (2014).

[20] A. Nagashima, N. Tejima, and C. Oshima, Phys. Rev. B **50**, 17487 (1994).

[21] C. Virojanadara, S. Watcharinyanon, A. A. Zakharov, and L. I. Johansson, Phys. Rev. B **82**, 205402 (2010).

[22] S. Schumacher, T. O. Wehling, P. Lazic, S. Runte, D. F. Forster, C. Busse, M. Petrovic, M. Kralj, S. Blugel, N. Atodiresei, V. Caciuc, and T. Michely, Nano Lett. **13**, 5013 (2013).

[23] M. Petrović, I. S. Rakić, S. Runte, C. Busse, J. T. Sadowski, P. Lazić, I. Pletikosić, Z.-H. Pan, M. Milun, P. Pervan, N. Atodiresei, R. Brako, D. Šokčević, T. Valla, T. Michely, and M. Kralj, Nat. Commun. **4**, 2772 (2013).

[24] A. L. Walter, K.-J. Jeon, A. Bostwick, F. Speck, M. Ostler, T. Seyller, L. Moreschini, Y. S. Kim, Y. J. Chang, K. Horn, and E. Rotenberg, Appl. Phys. Lett. **98**, 184102 (2011).

[25] C. Herbig, M. Kaiser, N. Bendiab, S. Schumacher, D. F. Förster, J. Coraux, K. Meerholz, T. Michely, and C. Busse, J. Phys.: Condens. Matter **24**, 314208 (2012).

[26] N. A. Vinogradov, K. A. Simonov, A. V. Generalov, A. S. Vinogradov, D. V. Vyalikh, C. Laubschat, N. Mårtensson, and A. B. Preobrajenski, J. Phys.: Condens. Matter **24**, 314202 (2012).

[27] Y. Zhang, Q. Fu, Y. Cui, R. Mu, L. Jin, and X. Bao, Phys. Chem. Chem. Phys. **15**, 19042 (2013).

[28] S. Lizzit, R. Larciprete, P. Lacovig, M. Dalmiglio, F. Orlando, A. Baraldi, L. Gammelgaard, L. Barreto, M. Bianchi, E. Perkins, and P. Hofmann, Nano Lett. **12**, 4503 (2012).

[29] E. Grånäs, U. Schroeder, M. A. Arman, M. Andersen, T. Gerber, K. Schulte, J. N. Andersen, B. Hammer, T. Michely, and J. Knudsen (unpublished).

[30] B. Smit and T. L. M. Maesen, Nature **451**, 671 (2008).

[31] X. Pan and X. Bao, Chem. Commun., 6271 (2008).

[32] J. Enkovaara, C. Rostgaard, J. J. Mortensen, J. Chen, M. Dułak, L. Ferrighi, J. Gavnholt, C. Glinsvad, V. Haikola, H. A. Hansen, H. H. Kristoffersen, M. Kuisma, A. H. Larsen, L. Lehtovaara, M. Ljungberg, O. Lopez-Acevedo, P. G. Moses, J. Ojanen, T. Olsen, V. Petzold, N. A. Romero, J. Stausholm-Møller, M. Strange, G. A. Tritsaris, M. Vanin, M. Walter, B. Hammer, H. Häkkinen, G. K. H. Madsen, R. M. Nieminen, J. K. Nørskov, M. Puska, T. T. Rantala, J. Schiøtz, K. S. Thygesen, and K. W. Jacobsen, J. Phys.: Condens. Matter **22**, 253202 (2010).

[33] S. R. Bahn and K. W. Jacobsen, Comput. Sci. Eng. **4**, 56 (2002).

[34] J. Klimeš, D. R. Bowler, and A. Michaelides, J. Phys.: Condens. Matter **22**, 022201 (2010).

[35] F. Mittendorfer, A. Garhofer, J. Redinger, J. Klimes, J. Harl, and G. Kresse, Phys. Rev. B **84**, 201401 (2011).

[36] W. Liu, J. Carrasco, B. Santra, A. Michaelides, M. Scheffler, and A. Tkatchenko, Phys. Rev. B **86**, 245405 (2012).

[37] L. B. Vilhelmsen and B. Hammer, Phys. Rev. Lett. **108**, 126101 (2012).

[38] L. B. Vilhelmsen and B. Hammer, J. Chem. Phys. **141**, 044711 (2014).

[39] D. Hagen, B. Nieuwenhuys, G. Rovida, and G. Somorjai, Surf. Sci. **57**, 632 (1976).

[40] M. Bianchi, D. Cassese, A. Cavallin, R. Comin, F. Orlando, L. Postregna, E. Golfetto, S. Lizzit, and A. Baraldi, New J. Phys. **11**, 063002 (2009).

[41] H. Zhang, A. Soon, B. Delley, and C. Stampfl, Phys. Rev. B **78**, 045436 (2008).

[42] C. M. Comrie and W. H. Weinberg, J. Chem. Phys. **64**, 250 (1976).

[43] L.-M. Yang and S.-L. Yau, J. Phys. Chem. B **104**, 1769 (2000).

[44] W. P. Krekelberg, J. Greeley, and M. Mavrikakis, J. Phys. Chem. B **108**, 987 (2004).

[45] C. J. Hagedorn, M. J. Weiss, and W. H. Weinberg, Phys. Rev. B **60**, R14016 (1999).

[46] M. Bianchi, E. D. L. Rienks, S. Lizzit, A. Baraldi, R. Balog, L. Hornekær, and P. Hofmann, Phys. Rev. B **81**, 041403 (2010).

[47] T. Langer, D. F. Förster, C. Busse, T. Michely, H. Pfnür, and C. Tegenkamp, New J. Phys. **13**, 053006 (2011).